Plasma chemistry of $He/O_2/SiH_4$ and $He/N_2O/SiH_4$ mixtures for remote plasma-activated chemical-vapor deposition of silicon dioxide

Mark J. Kushner
University of Illinois, Department of Electrical and Computer Engineering, 1406 West Green Street, Urbana, Illinois 61801

(Received 23 April 1993; accepted for publication 24 August 1993)

Remote plasma-activated chemical-vapor deposition (RPACVD) provides a means to deposit thin dielectric films with low ion bombardment and while having high selectivity in generating precursors. In RPACVD of SiO_2, gas mixtures of He/O_2 or He/N_2O are passed through a plasma, producing radicals and excited states that are mixed with silane downstream. Excited states produced in the plasma and precursor species produced by these reactions then flow to the substrate. Although high-quality SiO_2 films can be produced by RPACVD, the gas-phase deposition precursors have not been identified. A two-dimensional plasma chemistry model is described, and results from that model are used in a discussion of possible gas-phase precursors for SiO_2 deposition. In particular, the formation and transport of silanols (SiH_2O and SiH_3O) are examined as a function of gas mixture, power deposition, and geometry. It is found that the fluxes of SiH_2O, SiH_3O, and SiH_3 are sufficient to account for the observed deposition rates; while systematic dependencies of the fluxes of HSiO and SiO discount them as being deposition precursors. $He/N_2O/SiH_4$ mixtures differ from $He/O_2/SiH_4$ mixtures by providing larger fluxes of SiH_3 to the substrate, while the fluxes of SiH_2O, SiH_3O, and $O_2(^1\Delta)$ are significantly less.

I. INTRODUCTION

The low thermal budgets now encountered in microelectronics fabrication have motivated the development of plasma-enhanced chemical-vapor-deposition (PECVD) processes for laying down thin films of silicon dioxide at low temperatures in deferance to thermal chemical-vapor deposition.[1] PECVD of SiO_2 is commonly performed in low-pressure radio-frequency (rf) or microwave discharges sustained in mixtures of SiH_4/O_2 and SiH_4/N_2O.[2–8] In traditional PECVD using rf plasmas, the substrate is located in the plasma, typically on one of the electrodes. As a result, the substrate is subject to energetic particle bombardment which may damage the wafer. Also, since all of the feedstock gases are flowed through the plasma, one has little control over the reaction pathways.

To address these problems, remote plasma-activated chemical-vapor deposition (RPACVD) was developed.[9] In RPACVD the substrate is located downstream of the plasma zone (see Fig. 1). Nonreactive gases (or a subset of the deposition gases) are flowed through the plasma zone. Excited states and radicals flow into a downstream chamber where the (remaining) deposition gases are injected. Excitation transfer and chemical reactions between the activated gases and the injected gases then produce the deposition precursors. By placing the substrate outside the plasma zone, this method reduces the potential to damage the wafer. Since the deposition gases are not flowed through the plasma zone, a greater degree of control over production of radicals is also possible. RPACVD has successfully been used to fabricate thin films of *a*-Si:H, μc-Si, *c*-Si, SiO_2, Si_3N_4, and III-V compounds.[9]

In this article our interest is in the use of RPACVD to fabricate SiO_2 films. In these processes, developed by Lucovsky *et al.*,[10–20] mixtures of He/O_2 or He/N_2O are flowed through the plasma zone and SiH_4 is injected downstream. Reactions between the activated gases and the SiH_4 produce the deposition precursors. Gas pressures are typically 100–300 mTorr at flow rates of 100–400 sccm, resulting in residence times in the reactor of tens to hundreds ms. A schematic of a typical RPACVD reactor is shown in Fig. 1. The plasma is sustained in a narrow tube upstream, usually by a rf discharge (13.56 MHz). Excited states and ions of helium are rapidly quenched in the plasma zone by reactions with O_2 or N_2O producing O atoms, or are quenched on the walls. O atoms and excited states of O_2 are also produced by electron impact. The activated species which flow downstream and are mixed with SiH_4 are therefore primarily excited states and fragments of O_2 and N_2O. The gas mixtures typically consist of 1%–20% O_2 in He, with $<1\%$ SiH_4 injected downstream. This produces deposition rates for SiO_2 of many to 100 Å s^{-1}. For a given power deposition, the deposition rate using He/O_2 is usually greater than using He/N_2O.

In spite of the increasing use of RPACVD of SiO_2 in fabricating microelectronics devices,[9] the deposition precursors and reaction pathways are still being debated, thereby making optimization of the system by other than empirical methods difficult. To investigate the reaction pathways and to identify deposition precursors, a model has been developed for the RPACVD of SiO_2 using $He/O_2/SiH_4$ and $He/N_2O/SiH_4$ chemistries. The model accounts for the plasma and neutral chemistry of He/O_2- or He/N_2O-activated systems where SiH_4 is injected downstream. This investigation makes use of a previously described model for the RPACVD of *a*-Si:H and Si_3N_4 using $He/NH_3/SiH_4$ chemistries.[21]

The mechanics of the model are described in Sec. II, followed by a discussion of the important chemical reactions and possible deposition precursors in Sec. III. Results

 0021-8979/93/74(11)/6538/16/$6.00 © 1993 American Institute of Physics

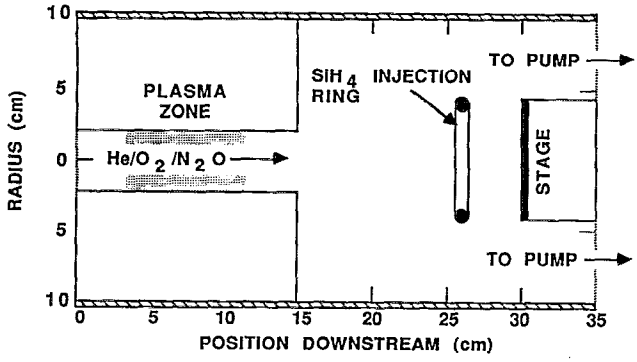

FIG. 1. Schematic of experimental RPACVD reactor. The plasma is sustained in the narrow tube at the top. Nondeposition gases, or a subset of the required deposition gases, are flowed through the plasma zone and into the lower mixing chamber. Additional deposition gases are injected through dispersal rings in the lower chamber.

from the model are discussed in Sec. IV, followed by concluding remarks in Sec. V.

II. DESCRIPTION OF THE MODEL

The model used in this study is functionally the same as that described in Ref. 21, and therefore will be only briefly described here. The model is a two-dimensional (cylindrically symmetric) simulation of the electron kinetics and plasma chemistry in a RPACVD reactor. A schematic of the model reactor is shown in Fig. 1. A subset of the gases is passed through the narrow portion of the reactor and flow into larger deposition chamber downstream. Other deposition gases are injected downstream through circular nozzles. In the cases considered here, mixtures of He/O_2 or He/N_2O are flowed through the plasma zone, while SiH_4 is injected from the nozzles. The plasma is sustained in the narrow upper portion of the reactor by a rf discharge. This arrangement corresponds to the "plasma confined" mode of RPACVD.[9]

Electron-impact rate coefficients for the plasma chemistry model are obtained from a companion Monte Carlo simulation for the gas mixture of interest, and parameterized as a function of the average electric field in the plasma. Tables of electron-impact rate coefficients are then interpolated during the simulation based on a specified power deposition. The advective flow field is separately computed and used for all species. Continuity equations including advection, diffusion, and gas-phase chemistry are formulated for all species, couched in finite difference form, and integrated in time using a third-order Runga–Kutta scheme. Due to the vastly different kinetic time scales for reactions in the plasma zone compared to downstream locations; and for kinetic reactions compared to convection, a time slicing technique is used. The local kinetics portions of the continuity equations are separately integrated for each spatial location for a dynamically selected Δt using (smaller) time steps as appropriate for each mesh point. This integration is then followed by a single reactor-wide integration of the convection portion of the continuity equations. Surface reactions are included as boundary conditions to the transport equations. Reactive sticking coefficients and products are specified for all species. Products of wall reactions are included as fluxes entering the plasma from the wall or substrate.

III. DESCRIPTION OF THE REACTION CHEMISTRY

In this section the reaction chemistry of $He/O_2/SiH_4$ and $He/N_2O/SiH_4$ plasma-activated gas mixtures is discussed. The species included in the model are listed in Table I. The reaction chemistry of activated NH_n and SiH_n is discussed in Ref. 21 in the context of RPACVD of Si_3N_4 using $He/SiH_4/NH_3$ mixtures. The reaction chemistry of He/SiH_4 mixtures is discussed in Ref. 22 in the context of PECVD of *a*-Si:H and updated in Ref. 21. For brevity, a discussion and listing of reactions in He/SiH_4 mixtures will not be repeated here. We will discuss, and list in Table II, reactions and mechanisms for the addition of O_2 and N_2O to He/SiH_4 gas mixtures.

A. Electron-impact processes

The electron kinetics reaction scheme for He/SiH_4 mixtures discussed in Refs. 21 and 22 was also used here. Minor revisions to that reaction scheme were made with recently available reaction rate coefficients for ion-molecule reactions from Reents and Mandich.[49]

The electron-impact processes in N_2O discharges were recently reviewed by Kline *et al.*[27] and the reactions we used in this work are listed in Table II. The cross sections we used for N_2O were taken from Hayashi and Niwawi,[26] with branchings for dissociative processes coming from Kline *et al.*[27] Electron-impact dissociation of N_2O separately produces $O(^1D)$ and $N_2(A)$ with branchings of 0.1 each. Since both $O(^1D)$ and $N_2(A)$ are subsequently reactive with SiH_4 these branchings take on added importance. The electron-impact ionization of N_2O produces N_2O^+ with a branching of 0.92 with a minor branching to NO^+. The vibrational excitation of N_2O may be an important process in the formation of deposition precursors, and is discussed in more detail below.

The electron-impact processes for O_2 are discussed in Ref. 23, and those cross sections were used. The important branchings are for dissociative excitation producing $O(^1D)$ and $O(^3P)$. Following the work of Eliasson and Kogelschatz,[24] we assigned the dissociative electronic excitations with thresholds at 8.4 eV to have branchings to $O(^1D)+O(^3P)$, and those with thresholds at 6 eV to have branchings to $2\cdot O(^3P)$.

B. Neutral reaction chemistry

The reaction scheme for $He/SiH_4/NH_3$ mixtures discussed in Ref. 21 has been used here, as appropriate, with changes noted below. The reaction chemistry of $SiH_4/O_2/N_2O$ in low-pressure plasmas in the context of SiO_2 deposition is surprisingly uncertain in light of the considerable work that has been completed on silane combustion. The source of much of this uncertainty is the identity of the deposition precursors which, to our knowledge, have not been directly measured.

TABLE I. Species used in the model.

Rare gases and electrons						
He	He*	He^+	e			
Hydrogen species						
H_2	H_2^+	H_3^+	H	H^+	H^-	
Silane species						
SiH_4	$SiH_4(v1,3)$	$SiH_4(v2,4)$	Si_2H_6	Si_3H_8	Si_4H_{10}	Si_5H_{12}
Si	SiH	SiH_2	SiH_3			
Si_2H_2	Si_2H_3	Si_2H_4	Si_2H_5	Si_3H_7	Si_4H_9	Si_5H_{11}
SiH_3^+	SiH_2^+	SiH^+	Si^+			
$Si_2H_7^+$	$Si_2H_5^+$	$Si_2H_4^+$	$Si_2H_3^+$	$Si_2H_2^+$	$Si_3H_4^+$	
$Si_3H_6^+$	$Si_3H_7^+$	$Si_3H_5^+$	$Si_4H_6^+$	$Si_4H_8^+$	$Si_4H_{11}^+$	$Si_5H_{10}^+$
SiH_2^-	SiH_3^-					
Silane-nitrogen species						
$SiH_2(NH_2)$	$SiH(NH_2)_2$	$Si(NH_2)_3$				
$SiH_3(NH_2)$	$SiH_2(NH_2)_2$	$SiH(NH_2)_3$	$Si(NH_2)_4$			
SiN	SiN_2					
SiH_4N^+	SiH_3N^+	SiH_2N^+				
Silane-oxygen species						
SiH_3O	SiH_2O	HSiO	SiO	SiO_2		
Nitrogen and ammonia species						
NH_3	NH_2	NH	N	N^+		
N_2	$N_2(v<8)$	$N_2(v>8)$	N_2^+			
$N_2(A)$	$N(^4D)$	NNH	N_2H_2	N_2H_4		
NH_2^+	NH_3^+	NH_4^+				
N_2O	$N_2O(v=1-3)$	NO	NO_2	N_2O^+	NO^+	
Oxygen species						
O_2	$O_2(^1\Delta)$	O_2^{**}	O_2^+	O^+	O^-	
O	$O(^1D)$					
H_2O	OH	HO_2	H_2O_2			

To produce stoichiometric SiO_2 films, the gas mixtures are typically lean in SiH_4. In RPACVD, SiH_4 is typically not flowed directly through the plasma zone. The end result is that the majority of electron-impact processes in the plasma zone produce radicals such as O atoms which oxidize SiH_4, as opposed to fragmenting SiH_4 directly. Given these conditions, our discussion on reaction mechanisms will emphasize the oxidation pathways.

In thermal CVD there is evidence that silanols such as SiH_3OH are the deposition precursors. Experiments and modeling by Guinta, Chapple-Sokol, and Gordon[50] of thermal CVD of SiO_2 using SiH_4/N_2O and Si_2H_6/N_2O mixtures revealed a close correlation between deposition profiles and predicted SiH_3OH fluxes. A likely reaction sequence for thermal CVD is

$$N_2O+M \rightarrow O+N_2+M, \quad (1)$$

$$O+SiH_4 \rightarrow OH+SiH_3, \quad (2)$$

$$SiH_3+N_2O \rightarrow SiH_3O+N_2, \quad (3)$$

$$SiH_3O+SiH_4 \rightarrow SiH_3OH+SiH_3, \quad (4)$$

$$SiH_4 \rightarrow SiH_2+H_2, \quad (5)$$

$$SiH_2+N_2O \rightarrow SiH_2O+N_2. \quad (6)$$

Guinta and co-workers acknowledge that silanol (SiH_3OH) is a few oxidation steps away from SiO_2: however, it satisfies many of the requirements for a deposition precursor in terms of rate of production and reactivity. Silanone (SiH_2O) is also suggested as a precursor on the basis that it will stick to the growth surface where it will be further oxidized. This mechanism requires, then, an abundant flux of O and OH radicals to the surface to complete the oxidation. In conventional PECVD using SiH_4/N_2O mixtures, Smith[51] has found that silanol molecules such as $Si(OH)_4$ make only minor contributions to the film compared to other precursors such as SiO_n, SiH_n, O, or OH.

Pai *et al.*[19] proposed that SiH_2O, SiH_3O and silanol complexes such as $(SiH_3O)_2$ are likely deposition precursors. Later, using appearance potential mass spectrometry and He/O_2 activation, they did not detect significant densities of SiH_n fragments of SiH_4 in the downstream chamber. A measured decrease in the density of SiH_4 was attributed to consumption by film formation.[10] One may conclude that there is not significant fragmentation of SiH_4 to SiH_n by chemical reactions,[10] or that any fragments that are produced rapidly react to form other species.

Although gas-phase HSiO and SiO are products of the high-pressure combustion of SiH_4, their generation requires at least 3–4 sequential reactions with SiH_4 and its products. The short lifetimes of intermediates in low-temperature plasmas result in a low rate of production of these higher-order precursors, and so it is unlikely that the

TABLE II. Additional reactions for $He/SiH_4/N_2O/O_2$ mixtures.[a]

Process	Rate coefficient[b]	Ref.
Electron impact and recombination		
$e+O_2 \rightarrow O_2+e$	c	23
$e+O_2 \rightarrow O_2(v)+e$	c	23
$e+O_2 \rightarrow O^-+O$	c	23
$e+O_2 \rightarrow O_2(^1\Delta)+e$	c	23,24
$e+O_2 \rightarrow O_2^{**}+e$	c	23
$e+O_2 \rightarrow O(^1D)+O+e$	c	23
$e+O_2 \rightarrow O+O+e$	c	23
$e+O_2 \rightarrow O_2^++e+e$	c	23
$e+N_2 \rightarrow N_2+e$	c	25
$e+N_2 \rightarrow N_2(v<8)+e$	c	25
$e+N_2 \rightarrow N_2(A)+e$	c	25,d
$e+N_2 \rightarrow N+N+e$	c	25
$e+N_2 \rightarrow N_2^++e+e$	c	25
$e+N_2O(v>0) \rightarrow N_2O+e$	c	26
$e+N_2O(v>0) \rightarrow N_2+O^-$	c	26
$e+N_2O \rightleftarrows N_2O(1<v<3)+e$	c	26,e
$e+N_2O(v>0) \rightarrow N_2+O+e$	c	26,27,f
$e+N_2O(v>0) \rightarrow N_2O^++e+e$	c	26,27,f
$e+N_2O(v>0) \rightarrow NO^++N+e+e$	c	26,27,f
$e+N_2O(v>0) \rightarrow O^++N_2+e+e$	c	26,27,f
$e+N_2O(v>0) \rightarrow N_2^++O+e+e$	c	26,27,f
$e+N_2O(v>0) \rightarrow N^++NO+e+e$	c	26,27,f
$e+N_2O(v>0) \rightarrow N_2+O(^1D)+e$	c	26,27,f
$e+N_2O(v>0) \rightarrow N_2(A)+O+e$	c	26,27,f
$e+O_2^+ \rightarrow O+O(^1D)$	$1.00(-7)/T_e^{0.5}$	28,g,h
$e+N_2^+ \rightarrow N(^4D)+N$	$2.00(-7)/T_e^{0.5}$	28
$e+NO^+ \rightarrow N(^4D)+O$	$1.57(-7)/T_e^{0.5}$	g,h,i,28,29
$e+NO^+ \rightarrow N+O(^1D)$	$4.30(-8)/T_e^{0.5}$	g,h,i,28,29
$e+N_2O^+ \rightarrow N_2+O(^1D)$	$1.13(-7)/T_e^{0.5}$	g,h,i,28,29
$e+N_2O^+ \rightarrow N_2(A)+O$	$5.18(-8)/T_e^{0.5}$	g,h,i,28,29
$e+N_2O^+ \rightarrow N_2+O$	$3.50(-8)/T_e^{0.5}$	g,h,i,28,29
$M^++N^- \rightarrow M+N$	$1.00(-7)$	h,j,30
Oxygen-hydrogen-nitrogen		
$O+O_2^{**} \rightarrow O+O_2(^1\Delta)$	$3.00(-12)$	31
$O(^1D)+O_2 \rightarrow O_2(^1\Delta)+O$	$7.98(-13)\exp(680/T)$	31
$O+O+M \rightarrow O_2+M$	$5.00(-33)$ $cm^6\,s^{-1}$	27
$O_2(^1\Delta)+O_2 \rightarrow O_2+O_2$	$1.60(-18)$	31
$O_2^{**}+O_2 \rightarrow O_2(^1\Delta)+O$	$3.97(-16)$	31
$O_2^{**}+O_2 \rightarrow O_2+O_2$	$1.00(-16)$	31
$O+O_2(^1\Delta) \rightarrow O+O_2$	$1.30(-16)$	31
$O+NO_2 \rightarrow NO+O_2$	$9.30(-12)$	27
$O+NO+M \rightarrow NO_2+M$	$1.10(-31)$ $cm^6\,s^{-1}$	27
$O+N_2+M \rightarrow N_2O+M$	$5.00(-38)$ $cm^6\,s^{-1}$	27
$O+N+M \rightarrow NO+M$	$9.00(-33)$ $cm^6\,s^{-1}$	27
$O(^1D)+H_2O \rightarrow OH+OH$	$2.20(-10)$	32
$O(^1D)+N_2O(v>0) \rightarrow NO+NO$	$7.20(-11)$	27
$O(^1D)+N_2O(v>0) \rightarrow N_2+O_2$	$4.80(-11)$	27
$O(^1D)+NO \rightarrow O+NO$	$1.50(-10)$	27
$O(^1D)+N_2 \rightarrow O+N_2$	$3.00(-11)$	27
$O+OH \rightarrow H+O_2$	$7.50(-10)\exp(-30/T)/T^{0.5}$	33
$O+HO_2 \rightarrow OH+O_2$	$2.90(-11)\exp(200/T)$	33
$O+H_2 \rightarrow OH+H$	$3.44(-10)\exp(-6909.5/T)$	34
$O+H_2O \rightarrow OH+OH$	$6.14(-11)\exp(-8706/T)$	35
$OH+OH \rightarrow H_2O+O$	$3.50(-16)T^{1.4}\exp(200/T)$	33
$OH+OH+M \rightarrow H_2O_2+M$	$2.79(-21)\exp(-534.3/T)/T^{3.6}$ $cm^6\,s^{-1}$	35
$OH+H_2 \rightarrow H_2O+H$	$5.25(-17)T^{1.8}\exp(-1522.6/T)$	34
$OH+H \rightarrow O+H_2$	$1.48(-10)\exp(-5856.9/T)$	34
$OH+H+M \rightarrow H_2O+M$	$6.10(-26)/T^2$ $cm^6\,s^{-1}$	34
$OH+HO_2 \rightarrow H_2O+O_2$	$8.31(-11)$	34
$OH+H_2O_2 \rightarrow HO_2+H_2O$	$1.69(-11)\exp(-954.8/T)$	34
$HO_2+HO_2 \rightarrow H_2O_2+O_2$	$3.36(-12)$	34
$H+H+M \rightarrow H_2+M$	$1.80(-30)/T$ $cm^6\,s^{-1}$	34
$H+O_2 \rightarrow OH+O$	$1.99(-7)/T^{0.91}$	36
$H+O_2+M \rightarrow HO_2+M$	$8.83(-30)/T$ $cm^6\,s^{-1}$	34
$H+HO_2 \rightarrow H_2+O_2$	$4.20(-11)\exp(-351.8/T)$	34

TABLE II. (*Continued.*)

Process	Rate coefficient[b]	Ref.
Electron impact and recombination		
$H+HO_2 \rightarrow OH+OH$	$8.97(-10)\exp(-904.5/T)$	34
$H+H_2O_2 \rightarrow H_2+HO_2$	$3.68(-12)\exp(-603/T)$	34
$N(^4D)+N \rightarrow N+N$	$1.00(-11)$	37
$N(^4D)+N_2 \rightarrow N+N_2$	$2.00(-16)$	37
$N+N+M \rightarrow N_2+M$	$1.00(-32)$ $cm^6\,s^{-1}$	27,37
$N+N+M \rightarrow N_2(A)+M$	$2.33(-33)$ $cm^6\,s^{-1}$	37
$N+NO \rightarrow N_2+O$	$3.10(-11)$	27
$N_2(A)+N_2(A) \rightarrow N_2(A)+N_2$	$1.36(-9)$	38
$N_2(A)+N_2 \rightarrow N_2+N_2$	$1.90(-13)$	38
$N_2(A)+N \rightarrow N_2+N(^4D)$	$5.00(-11)$	37
$N_2(A)+N_2O(v\geq 0) \rightarrow N_2+N_2+O$	$7.70(-12)$	27,39
$N_2(A)+O_2 \rightarrow N_2+O+O$	$2.40(-12)$	27
$N_2(A)+NO \rightarrow N_2+NO$	$1.50(-11)$	27
Rare-gas excitation and charge transfer		
$He^*+N_2 \rightarrow N_2^+ +He+e$	$7.50(-11)$	40
$He^*+N_2O(v\geq 0) \rightarrow N_2O^+ +He+e$	$6.45(-10)$	41,k
$He^*+O_2 \rightarrow O_2^+ +He+e$	$2.54(-10)$	41,k
$He^+ +O_2 \rightarrow O^+ +O+He$	$1.07(-9)$	42
$He^+ +O_2 \rightarrow O_2^+ +He$	$3.30(-11)$	42
$He^+ +N_2O(v\geq 0) \rightarrow N_2O^+ +He$	$3.00(-10)$	42,h
$He^+ +N_2 \rightarrow N^+ +N+He$	$9.60(-10)$	42
$He^+ +N_2 \rightarrow N_2^+ +He$	$6.40(-10)$	42
$N_2^+ +N_2O(v\geq 0) \rightarrow N_2O^+ +N_2$	$7.00(-10)$	27
$N_2^+ +SiH_4 \rightarrow SiH_3^+ +N_2+H$	$1.00(-10)$	h
$O^+ +N_2O(v\geq 0) \rightarrow N_2O^+ +O$	$3.10(-10)$	27
$O^+ +N_2O(v\geq 0) \rightarrow NO^+ +NO$	$3.20(-10)$	27
$O^+ +SiH_4 \rightarrow SiH_2^+ +H_2+O$	$2.00(-10)$	h
$O_2^+ +SiH_4 \rightarrow SiH_2^+ +H_2+O_2$	$2.00(-10)$	h
$N_2O^+ +SiH_4 \rightarrow SiH_2^+ +H_2+N_2O$	$2.00(-10)$	h
N_2O vibrational kinetics		
$N_2O(v1)+M \rightleftarrows N_2O(v3)+M$	$1.00(-12)$	e,h
$N_2O(v3)+M \rightleftarrows N_2O(v2)+M$	$1.00(-12)$	e,h
$N_2O(v2)+M \rightleftarrows N_2O+M$	$1.00(-12)$	e,h
$N_2O(v1)+M \rightleftarrows N_2O(v2)+M$	$1.00(-12)$	e,h
$N_2O(v1)+M \rightleftarrows N_2O(v2)+M$	$1.00(-12)$	e,h
$N_2O(v3)+M \rightleftarrows N_2O+M$	$1.00(-12)$	e,h
Silane-nitrogen reactions		
$SiH_4+N(^4D) \rightarrow SiH_3+NH$	$5.70(-11)$	43
$SiH_4+N_2(v>8) \rightarrow SiH_2+H_2+N_2$	$2.70(-12)$	37
$SiH_4+N_2(A) \rightarrow SiH_3+H+N_2$	$5.00(-12)$	43,k
$SiH_4+N_2(A) \rightarrow SiH_2+H_2+N_2$	$5.00(-12)$	43,k
$SiH_2+N \rightarrow SiN+H_2$	$1.00(-10)$	37
$SiN+N \rightarrow Si+N_2(v>8)$	$6.60(-11)$	37
$SiH+N \rightarrow Si+N_2$	$3.30(-11)$	37
$Si+N_2+M \rightarrow SiN_2+M$	$6.60(-32)$ $cm^6\,s^{-1}$	37
$SiN_2+N \rightarrow SiN+N_2(v>8)$	$6.60(-11)$	37
$SiN_2+N \rightarrow SiN+N_2$	$3.30(-11)$	37
Silane oxidation		
$SiH_4+O \rightarrow SiH_3+OH$	$6.98(-12)\exp(-804/T)$	34,44
$SiH_4+O(^1D) \rightarrow OH+SiH_3$	$3.00(-10)$	45
$SiH_4+OH \rightarrow SiH_3+H_2O$	$1.40(-11)\exp(-50.3/T)$	34
$SiH_4+HO_2 \rightarrow SiH_3+H_2$	$4.98(-12)\exp(-2814.1/T)$	34
$SiH_4+O_2(^1\Delta) \rightarrow SiH_3O+OH$	0–$5.00(-12)$	h
$SiH_4+O_2^{**} \rightarrow SiH_3O+OH$	$5.00(-12)$	h
$SiH_3+O \rightarrow SiH_2O+H$	$2.16(-10)\exp(-1005/T)$	34
$SiH_3+OH \rightarrow SiH_2O+H_2$	$8.31(-12)$	34
$SiH_3+OH \rightarrow SiH_4+O$	$8.84(-14)\exp(-6540.8/T)$	34
$SiH_3+O_2 \rightarrow SiH_2O+OH$	$0.63(-11)$	34,29
$SiH_3+O_2 \rightarrow SiH_3O+O$	$0.63(-11)$	34,29
$SiH_3+H_2O_2 \rightarrow SiH_4+HO_2$	$6.74(-13)\exp(-550.9/T)$	34
$SiH_3+N_2O(v\geq 1) \rightarrow SiH_3O+N_2$	0–$2.00(-11)$	h
$SiH_2+O_2 \rightarrow SiH_2O+O$	$3.75(-12)$	46,k
$SiH_2+O_2 \rightarrow HSiO+OH$	$3.75(-12)$	46,k

TABLE II. (*Continued.*)

Process	Rate coefficient[b]	Ref.
Electron impact and recombination		
$SiH_2+N_2O(v>0) \rightarrow SiO+H_2+OH$	$1.90(-12)$	47,k
$SiH+NO \rightarrow SiO+NH$	$2.50(-10)$	48
$SiH+O_2 \rightarrow SiO+OH$	$0.85(-10)$	48
$SiH+O_2 \rightarrow SiO_2+H$	$0.85(-10)$	48
$SiH_3O+O \rightarrow SiH_2O+OH$	$1.00(-12)$	h
$SiH_3O+OH \rightarrow SiH_2O+H_2O$	$1.00(-11)$	44,h
$SiH_2O+H \rightarrow HSiO+H_2$	$5.48(-10)\exp(-5276.4/T)$	34
$SiH_2O+O \rightarrow HSiO+OH$	$2.99(-11)\exp(-1547.7/T)$	34
$SiH_2O+OH \rightarrow HSiO+H_2O$	$1.25(-11)\exp(-85.4/T)$	34
$SiH_2O+HO_2 \rightarrow HSiO+H_2O_2$	$1.66(-12)\exp(-4020.1/T)$	34
$HSiO+H \rightarrow SiO+H_2$	$3.32(-10)$	34
$HSiO+O \rightarrow SiO+OH$	$1.66(-10)$	34
$HSiO+OH \rightarrow SiO+H_2O$	$1.66(-10)$	34
$HSiO+OH \rightarrow SiH_2O+HO_2$	$8.84(-14)\exp(-6540.8/T)$	34
$HSiO+O_2 \rightarrow SiO+HO_2$	$1.99(-10)\exp(-1998.5/T)$	34
$HSiO+H_2O_2 \rightarrow SiH_2O+HO_2$	$4.95(-13)\exp(-178/T)$	34
$SiO+OH \rightarrow SiO_2+H$	$6.65(-12)\exp(-2864.3/T)$	34
$SiO+O+M \rightarrow SiO_2+M$	$6.90(-33)\exp(-2300/T)$ cm^6 s^{-1}	34
$SiO+O_2 \rightarrow SiO_2+O$	$2.36(-10)\exp(-3266.3/T)$	34
$SiO+HO_2 \rightarrow HSiO+O_2$	$1.48(-10)\exp(-5856.9/T)$	34

[a]A detailed listing of rate coefficients for silane-hydrogen plasma chemistry can be found in Ref. 22, and for rare-gas/SiH_4/NH_3 mixtures (with revisions to SiH_4/H_2 chemistry) can be found in Ref. 21.
[b]$1(-10) \equiv 1\times10^{-10}$. Rate coefficients have units of cm^3 s^{-1} unless noted. T is the gas temperature (K).
[c]Rate coefficient was obtained by convolving the electron energy distribution with the cross section from the indicated reference.
[d]The electron-impact rate coefficients to all nondissociative electronic state of N_2 were summed, and used for excitation of $N_2(A)$. This state therefore represents the total electronic excitation density.
[e]The reverse reaction was obtained by detailed balance.
[f]Cross section is from Ref. 26, branching ratio from Ref. 27.
[g]T_e is the electron temperature in eV.
[h]Estimated, see text for discussion or reference for similar rate coefficients.
[i]Branching ratio from Ref. 29.
[j]This rate coefficient was used for all positive ion (M^+) and negative ion (N^-) neutralizations.
[k]Estimated branching; see text for discussion.

chain will progress to SiO. In high-temperature systems where pyrolysis of SiH_4 produces SiH_2, or in plasma systems where electron impact produces SiH_2, reactions with O_2 or N_2O can generate HSiO and SiO directly, thereby reducing the number of steps in the oxidation chain.

In RPACVD using $He/O_2/SiH_4$ mixtures, electron-impact dissociation and excitation of O_2 produce $O(^3P)$, $O(^1D)$, $O_2(^1\Delta)$, and $O_2(v)$. Reactions of O atoms with SiH_4 proceed by a series of H abstraction or elimination reactions,

$$O+SiH_4 \rightarrow SiH_3+OH, \quad (7)$$

$$O+SiH_3 \rightarrow SiH_2O+H, \quad (8)$$

$$OH+SiH_3 \rightarrow SiH_2O+H_2, \quad (9)$$

$$O+SiH_2O \rightarrow HSiO+OH, \quad (10)$$

$$O+HSiO \rightarrow SiO+OH, \quad (11)$$

$$SiO+O_2 \rightarrow SiO_2+O. \quad (12)$$

The initiating step has an activation energy of 1.6 kcal/mol for the reactant $O(^3P)$, but proceeds at a gas kinetic rate with $O(^1D)$. The production of H or OH at every step continues the reaction chain by back reacting with SiH_4 to produce silyle radicals

$$OH+SiH_4 \rightarrow SiH_3+H_2O, \quad (13)$$

$$H+SiH_4 \rightarrow SiH_3+H_2. \quad (14)$$

SiH_3O is not produced in this chain; however, it is likely that SiH_3O is rapidly produced by reactions of SiH_3 with O_2. The details of the reaction of SiH_3 with O_2 are, however, somewhat uncertain. Tokuhashi *et al.*[34] studied the oxidation of SiH_4 and assigned an activation energy of 11.4 kcal/mol to $SiH_3+O_2 \rightarrow SiH_2O+OH$. This value would effectively eliminate the reaction of SiH_3 with O_2 in low-temperature plasmas. Koshi *et al.*,[29] however, measured an only moderately constrained rate coefficient of 1.26×10^{-11} cm^3 s^{-1} for the reaction of SiH_3 with O_2. They suggest that the intermediate complex $SiH_3O_2^*$ decays into three reaction products (shown with their suggested branchings at 5 Torr),

$$O_2+SiH_3 \rightarrow SiH_3O_2^* \rightarrow SiH_3O+O, \quad b=0.16, \quad (15a)$$

$$\rightarrow SiH_2O+OH, \quad b=0.24, \quad (15b)$$

$$\rightarrow SiH_2O_2+H, \quad b=0.60. \quad (15c)$$

SiH_2O_2 is most likely produced in an excited state which may decay to, for example, SiH_2O+OH, $SiHO+H_2O$, or $H(OH)SiO+H$. Slagle, Bernhardt, and Goodman[52] mea-

sured a rate coefficient of $4.96\times10^{-12}\exp(275/T)$ for the reaction of SiH_3 with O_2 but were not able to distinguish product species. We used the rate coefficient measured by Tokuhashi *et al.*[34] for reactions of SiH_3+O_2 and took equal branchings to SiH_2O and SiH_3O. This results in a reasonable production of SiH_3O. Once generated, SiH_3O can react with O and OH to form SiH_2O,

$$SiH_3O+O\rightarrow SiH_2O+OH, \tag{16}$$

$$SiH_3O+OH\rightarrow SiH_2O+H_2O. \tag{17}$$

We estimated these rate coefficients to be 10^{-12} $cm^3\,s^{-1}$ and 10^{-11} $cm^3\,s^{-1}$, respectively.

The production of SiH_2 by electron impact or other processes considerably speeds the production of these precursors as silylene rapidly reacts with O_2.[34] Tokuashi *et al.* quote a single branching to HSiO for reactions of SiH_2 with O_2. The branching to SiH_2O is exothermic by 26.5 kcal/mol and so we chose equal branchings to HSiO and SiH_2O using the reaction rate coefficient quoted by Chu and co-workers.[46]

Tsu *et al.*[10] and Lucovsky, Tsu, and Markunas[53] have cited evidence that deposition rates of SiO_2 are not well correlated with O atom densities as inferred from optical emission spectroscopy of the plasma region using He/O_2 gas mixtures. Tsu and co-workers observed that emission of the 777.4 nm line of atomic O decreases with increasing O_2 partial pressure while, at high substrate temperature (400 °C), the deposition rate increases with increasing O_2 partial pressure.[11] When O_2 is added to a He/O_2 discharge, the electron energy distribution assumes an increasingly cutoff character. Under these conditions, dissociative excitation of O_2 most likely proceeds through the $O_2(A\,^3\Sigma_u^+)$ state, which produces $2\cdot O(^3P)$, and through the $O_2(B\,^3\Sigma_u^-)$ state which produces $O(^3P)$ and $O(^1D)$.[24] Lucovsky's observations could be explained by O atoms being produced and reacting dominantly in their ground states or low excited states; or other dark channels being important.

Large densities of the "dark species" $O_2(^1\Delta)$ and $O_2(v)$ are produced in the plasma zone of RPACVD reactors. It has been suggested that reaction of $O_2(^1\Delta)$ and SiH_4 on surfaces produce precursors which condense to form the SiO_2 film.[52] This suggestion motivates examination of whether $O_2(^1\Delta)$ reacts with SiH_4 in the gas phase as well. For example, the reaction

$$SiH_4+O_2(^1\Delta)\rightarrow SiH_3O+OH \tag{18}$$

is exothermic by 40 kcal/mol. There are no measurements of the rate coefficient of this reaction that we are aware of. We have parametrized the rate coefficient to a maximum value of 5×10^{-12} $cm^3\,s^{-1}$, and the results are discussed below. The importance of reactions of $O_2(v)$ with SiH_4 is somewhat in question. It is possible that successive *v-v* reactions of $O_2(v)$ to SiH_4 could result in pyrolysis of SiH_4,

$$O_2(v)+SiH_4(v)\rightarrow SiH_4(v'')+O_2, \tag{19}$$

$$SiH_4(v'')\rightarrow SiH_2+H_2, \tag{20}$$

however, 11 vibrational quanta would need to be transferred from $O_2(v)$ to SiH_4 for this to occur. That rate of excitation transfer is unlikely at low pressures.

There is considerable evidence that a surface catalyzed reaction may be important in RPACVD. For example, experiments have been performed where deposition was observed on a substrate which was separated from the plasma by stainless-steel wool plugs. The plugs would presumably pass only very long-lived species such as $O_2(^1\Delta)$. Lucovsky suggests that $O_2(^1\Delta)$ and excited silane may be the deposition precursors through a surface catalyzed reaction.[12] Since all observed electronic states of SiH_4 are dissociative, SiH_4^* can only be vibrationally excited silane. Due to the rapid rate of *V-T* reactions with O_2 which are characteristic of polyatomic molecules,[22] it is difficult to build up large densities of $SiH_4(v)$ in highly excited levels. Therefore, the $SiH_4(v)$ arriving at the substrate can contain only a few quanta of vibrational energy. Since the quenching probability for $SiH_4(v)$ is nearly unity at the surface, it is unlikely that the energy of $SiH_4(v)$ and $O_2(^1\Delta)$ can be added. Therefore, at low substrate temperatures where the rate of pyrolysis of SiH_4 is small, all the energy for producing the precursors must come from gas-phase $O_2(^1\Delta)$ reacting with silane adsorbed on the surface, denoted $SiH_4(a)$. Since, however, the internal energy of $O_2(^1\Delta)$ is only 0.98 eV, which is below the appearance potential for fragments of SiH_4, a surface reaction which is analogous to the gas-phase reaction in Eq. (18) must occur. That is, the surface catalyzed reaction produces a deposition precursor which then condenses to form the film

$$O_2(^1\Delta)+SiH_4(a)\rightarrow SiH_nO(a)\rightarrow \text{film}. \tag{21}$$

This mechanism would require that the gas-phase reaction in Eq. (18) have a small rate coefficient to ensure that $O_2(^1\Delta)$ is not otherwise depleted in the gas phase prior to reaching the substrate. Although $O_2(v)$ probably does not directly fragment SiH_4, it is certainly reasonable to expect that reactions of SiH_3 and SiH_2 with O_2 are enhanced if the latter reactant is vibrationally excited.

SiH_4/N_2O oxidation differs from SiH_4/O_2 primarily in the manner of producing the oxidizing agents. Electron-impact dissociation of N_2O produces O, N_2, $N_2(A)$, and $O(^1D)$. Since most fragments of SiH_4 are unreactive with N_2,[46] silane oxidation in SiH_4/N_2O mixtures proceeds in nearly the same fashion as in SiH_4/O_2. The exception is that $N_2(A)$ is quenched by silane in a dissociative excitation transfer. Piper and Caledonia[43] suggest that the products are either SiH_3 or SiH_2, and we have assigned equal branchings to each.

Small amounts of $N(^4D)$ are produced by dissociative excitation of N_2 and by dissociative recombination of NO^+ and N_2^+. Unlike $N(^4S)$, which is unreactive with SiH_4, the excited state will abstract H at approximately half the gas kinetic rate,[43]

$$SiH_4+N(^4D)\rightarrow SiH_3+NH, \quad k=5.7\times10^{-11}\ cm^3\,s^{-1}. \tag{22}$$

NH is, itself, unreactive with SiH_4.

The reactions of SiH_2 and SiH_3 with N_2O are potentially important processes in low-temperature SiH_4/N_2O systems. The electron-impact dissociation of N_2O in the discharge dominantly produces N_2+O. The O atoms then abstract O from SiH_4 producing SiH_3+OH. In the SiH_4/O_2 system, SiH_3 can then react with the feedstock O_2 to form SiH_3O+O, and thereby sustain the chain. This chain sustaining reaction may, in part, explain the larger deposition rate that can be produced in SiH_4/O_2 systems. In low-temperature SiH_4/N_2O systems there is no analogous reaction of SiH_3 with N_2O. Kinetics measurements by Slagle and co-workers[52] could not detect any reaction between SiH_3 and N_2O at room temperature, which is an unexpected result considering the reaction $SiH_3+N_2O\rightarrow SiH_3O+N_2$ is exothermic by 88 kcal/mol. Guinta and co-workers[50] estimated that the reaction has a rate coefficient of $1.5\times10^{-10}\exp(-18.0\text{ kcal mol}^{-1}/RT)$ $\text{cm}^3\text{ s}^{-1}$, which produces a negligible rate coefficient at near room temperature, in agreement with Slagle's results. It is difficult, however, to account for observed deposition rates of SiO_2, particularly in remote systems, without having a reaction of SiH_3 with the feedstock gases.

The electron-impact rate coefficients for vibrational excitation of N_2O are large. When using estimated rate coefficients for v-T relaxation of 10^{-12} cm^{-3}, we predict that a large density of $N_2O(v)$ flows downstream from the plasma zone. Although the first three vibrational modes of N_2O have energies of only 1.6–3.5 kcal/mol, which is small compared to the thermal activation energy estimated by Guinta and co-workers,[50] the ability of vibrationally excited species to speed reactions is well known. As a test reaction, we have estimated that

$$SiH_3+N_2O(v)\rightarrow SiH_3O+N_2 \tag{23}$$

proceeds with a rate coefficient of 2×10^{-11} $\text{cm}^3\text{ s}^{-1}$.

The reaction of $SiH_2+N_2O\rightarrow SiH_2O^*+N_2$ has a rate coefficient measured by Becerra *et al.*[47] of 1.9×10^{-12} $\text{cm}^3\text{ s}^{-1}$, and is exothermic by 107 kcal/mol. Becerra *et al.* suggest that the SiH_2O^* quickly decays, with one possible set of products being $SiO+H_2$. We have chosen this branching.

C. Excited-state and ion chemistry

The excited-state ion chemistry of $He/O_2/SiH_4$ and $He/N_2O/SiH_4$ mixtures is also poorly known. Penning reactions of He* with O_2 and N_2O produce ions, in what we have estimated to be nondissociative processes,

$$He^*+O_2\rightarrow O_2^++He+e,\quad k=2.54\times10^{-10}\text{ cm}^3\text{ s}^{-1}, \tag{24a}$$

$$+N_2O\rightarrow N_2O^++He+e,\quad k=6.45\times10^{-10}\text{ cm}^3\text{ s}^{-1}. \tag{24b}$$

Charge exchange of He^+ with O_2 produces both monomer and dimer ions,[42]

$$He^++O_2\rightarrow O_2^++He,\quad k=1.07\times10^{-9}\text{ cm}^3\text{ s}^{-1}, \tag{25a}$$

$$\rightarrow O^++O+He,\quad k=3.3\times10^{-11}\text{ cm}^3\text{ s}^{-1}. \tag{25b}$$

Charge exchange of He^+ with N_2O is estimated to have a rate coefficient of 3×10^{-10} $\text{cm}^3\text{ s}^{-1}$ with a single branching to N_2O^+. Charge-exchange reactions of O^+, N_2O^+, and O_2^+ with SiH_4 are exothermic for only the branching to $SiH_2^++H_2$. We have used this branching for all of these reactions, with an estimated rate coefficient of 2×10^{-10} $\text{cm}^3\text{ s}^{-1}$. The more energetic ion N_2^+ charge exchanges with SiH_4 with an estimated branching to SiH_3^+. Since RPACVD is typically performed by passing He/O_2 or He/N_2O mixtures through the plasma zone, only charge exchange of He^+ with O_2 or N_2O is significant since He^+ does not survive in large numbers to the downstream chamber. Unless silane back diffuses into the plasma zone, few helium-silane excitation transfer reactions take place.

Recombination of SiH_x^+ ions are discussed in Ref. 22. The recombination of O_2^+, NO^+, and N_2O^+ are dissociative. The following branchings for N_2O^+, as suggested by Johnson,[29] were used:

$$e+N_2O^+\rightarrow N_2+O(^1D),\quad b=0.566, \tag{26a}$$

$$\rightarrow N_2(A)+O,\quad b=0.259, \tag{26b}$$

$$\rightarrow N_2+O,\quad b=0.175. \tag{26c}$$

IV. PRECURSOR FLUXES IN RPACVD OF SiO_2

The test system is based on the RPACVD reactor of Lucovsky and co-workers,[53] schematically shown in Fig. 1. The plasma zone is 5 cm in diameter while the downstream deposition chamber is 20 cm in diameter and 20 cm long. He/O_2 or He/N_2O mixtures are flowed through the plasma zone and SiH_4 is injected through nozzles of adjustable height (2–10 cm) above the substrate (8 cm diameter). The standard conditions are a gas pressure of 300 mTorr and a total flow rate of 210 sccm. The average residence time is $\approx$50 ms. Power deposition is 0.3 W cm^{-3} in the plasma zone.

Our base case uses a gas mixture of $He/O_2/SiH_4=95/5/0.1$. The peak electron density in the plasma zone is $\approx1.9\times10^{11}$ cm^{-3} (see Fig. 2). The dominant ion for this case is O_2^+ (maximum density 1.2×10^{11} cm^{-3}), which is produced primarily by electron impact and secondarily by Penning ionization by He*. O^+ and He^+ are produced in approximately the same density ($3.5\text{–}4\times10^{10}$ cm^{-3}), with the former primarily being produced by charge exchange from He^+ to O_2. In this work we have assumed that the production of the plasma can be well confined to the narrow upstream zone. (Operation with an unconfined plasma will be addressed in a subsequent publication.) As a result, production of SiH_4 ions can only occur by electron impact of SiH_4 which back diffuses into the plasma zone or charge exchange (and Penning processes) downstream. Since He* and He^+ are rapidly quenched in the plasma zone by reactions with O_2, there are few ionizing excitation transfer reactions to SiH_4 from He* and He^+ downstream. Although O^+ and O_2^+ do charge exchange with SiH_4, their densities are fairly well depleted before encountering the injected SiH_4 downstream. The end result is that the production of SiH_n^+ ions is small, and is basically restricted to that resulting from

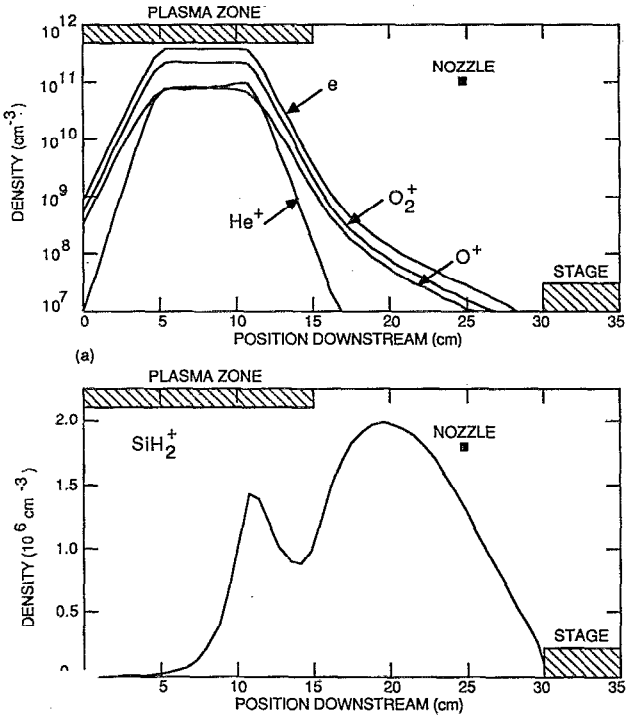

FIG. 2. Densities of electrons and select ions as a function of axial position (at $r=0$) for the base case conditions ($He/O_2/SiH_4=95/5/0.1$, 300 mTorr, 210 sccm): (a) e, O_2^+, O^+, He^+; (b) SiH_2^+.

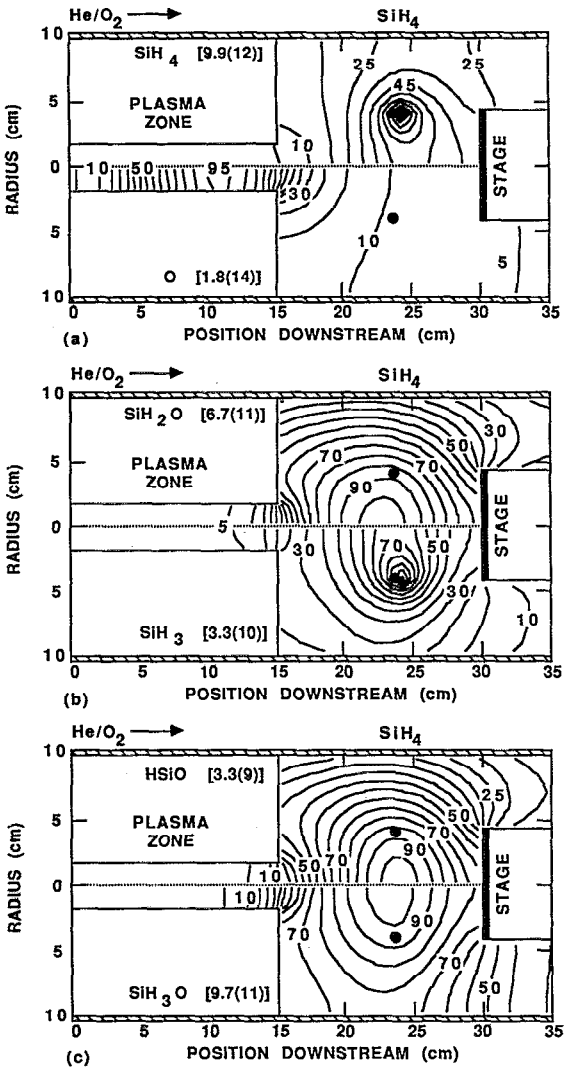

FIG. 3. Predicted densities of deposition precursors for the base case conditions ($He/O_2/SiH_4=95/5/0.1$, 300 mTorr, 210 sccm): (a) SiH_4 and O atoms; (b) SiH_2O and SiH_3; (c) HSiO and SiH_3O. He/O_2 is flowed through the plasma zone while SiH_4 is injected downstream from the circular nozzles. The SiH_3 is formed by H abstraction by O from SiH_4. The SiH_3O is formed primarily by reaction of SiH_3 with O_2. The number in brackets by the species label is the maximum density (cm^{-3}). The contour labels are the percent of the maximum value, where 1(9) denotes 1×10^9.

back diffusion of SiH_4 into the plasma zone. For example, the density of electrons and ions are shown in Fig. 2 for the base case conditions. SiH_2^+ is produced in the plasma zone due to back diffusion of SiH_4, and downstream by charge transfer from O^+ and O_2^+, but in very small numbers.

Operating in a confined plasma mode is more likely when moderate pressure (300 mTorr) He/O_2 mixtures are passed through the plasma zone, compared to passing low-pressure ($<$100 mTorr) He through the plasma zone and injecting O_2 downstream. This results from the fact that molecular ion plasmas generally decay more rapidly than rare-gas plasmas. The rate coefficient for dissociative recombination of O_2^+ is $>10^{-7}$ cm^{-3}, resulting in a recombination time of hundreds of μs to 1 ms, which is small compared to the gas residence time (tens to hundreds of ms); therefore, the plasma fails to penetrate far downstream. Volumetric recombination of the rare-gas ions at low pressure is slow and Penning reactions by rare-gas metastable continue to produce ions downstream. This results in a reasonable penetration of the plasma downstream.

The O atom and SiH_4 densities are shown in Fig. 3(a) for the base case.[54] O atoms are produced primarily by electron-impact dissociation of O_2. Due to the non-Maxwellian "cutoff" electron energy distribution, the amount of power that is dissipated in exciting and ionizing He is comparatively small, resulting in a small contribution of dissociative excitation transfer reactions from He^+ to the production of O atoms. The O_2 is $\approx$10%–15% dissociated in the plasma. O atoms recombine with $<1\%$ probability on Pyrex surfaces at near room temperature,[55] and so the majority of the O atoms generated in plasma (maximum density 9.5×10^{13} cm^{-3}) either flow downstream or back diffuse out of the plasma zone. The downstream O atom density [virtually all $O(^3P)$] is $1\text{–}3\times10^{13}$ cm^{-3}. $O(^1D)$ is produced by dissociative excitation of O_2, but is rapidly quenched by excitation transfer forming $O_2(^1\Delta)$ and does not penetrate far downstream as shown in Fig. 4(a). SiH_4 is injected from the nozzles, advects downstream, and back diffuses upstream. The moderate flow rate and narrow plasma zone prevents significant leakage of the SiH_4 into the plasma, which would compromise the selectivity of the RPACVD process.

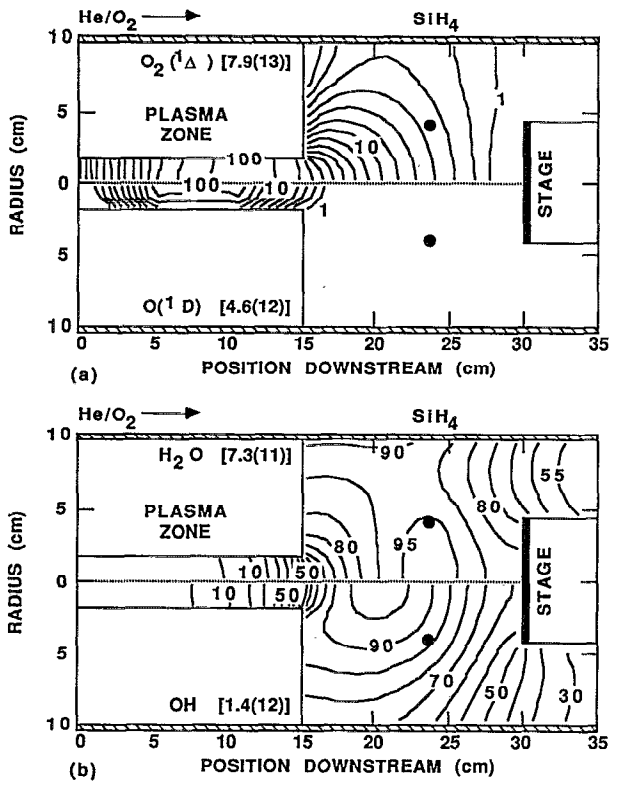

FIG. 4. Species densities for the conditions of Fig. 3: (a) $O_2(^1\Delta)$ and $O(^1D)$; (b) H_2O and OH. $O(^1D)$ is quickly quenched or converted to $O_2(^1\Delta)$, and does not penetrate downstream. H_2O is a product of OH reacting with SiH_nO, and accumulates in the chamber. (The labeling scheme is the same as Fig. 3.)

The reaction between O and SiH_4 is a moderately fast H abstraction process [Eq. (7)], producing SiH_3 whose density is shown in Fig. 3(b). The density of SiH_3 in the vicinity of the substrate is $\approx 10^{10}$ cm^{-3}. The spatial pattern of SiH_3 indicates that its production is rate limited by transport of SiH_4 and that its reaction with O_2 is sufficiently fast that it is consumed near the site of its generation. A small amount of leakage of SiH_4 into the plasma zone is indicated by the extended tail of SiH_3 in the throat of the plasma zone. SiH_3 at this location is produced by reactions with O atoms and electron-impact dissociation of SiH_4.

In our reaction scheme, SiH_3 reactions with O_2 produce SiH_2O and SiH_3O with equal branchings. SiH_2O can also be produced by H abstraction of O from SiH_3O. The densities of SiH_2O and SiH_3O are shown in Figs. 3(b) and 3(c). Our estimated reactive sticking coefficients on the cold reactor walls are 0.1 and 0.01 for SiH_2O and SiH_3O, respectively. These differences, and the somewhat higher reactivity of SiH_2O with O, explain the higher density of SiH_3O in the vicinity of the substrate ($\approx 6\times 10^{11}$ cm^{-3}) compared to SiH_2O (3×10^{11} cm^{-3}).

The production of HSiO is dominated by H abstraction by O from SiH_2O and reactions of SiH_2 with O_2. Its density, though, is only $\approx 2\times 10^9$ cm^{-3} in the vicinity of the substrate. This is partly a result of a low rate of production, and partly a result of its higher sticking coefficient (estimated to be 0.1). The gas-phase densities of SiO and SiO_2 are $< 10^9$ cm^{-3}.

The products of H abstraction by O and OH from SiH_nO_m are OH and H_2O, respectively, and these densities are shown in Fig. 4(b). OH is itself reactive with SiH_4 and will abstract H to form SiH_3. OH then represents a link in a short chain in producing SiH_3 and subsequently SiH_nO. H_2O is unreactive, and so accumulates in the chamber. The densities of both species are ≈ 5–6×10^{11} cm^{-3} in the vicinity of the substrate. This situation might cause concern since hydrogen can be incorporated into the film by reactions of ambient water with the surface,[14]

$$=\text{Si-O-Si}= + \text{H}_2\text{O} \rightarrow =\text{Si-OH} + =\text{Si=OH}. \quad (27)$$

Moderate substrate temperatures are therefore required to either prevent such intake or to eliminate =Si-O-H bonding brought to the surface by precursors. For example, films grown at 200 °C showed no significant =Si-O-H bonding while those at 100 °C did show =Si-O-H bonding.[14,55] One advantage of RPACVD compared to conventional PECVD is that a larger proportion of H_2O produced by these reactions can be directly pumped out of the chamber before striking the substrate, thereby reducing H incorporation.

It has been observed that the H content of SiO_2 films (in the form of =Si-OH bonding) increases with increasing deposition rate. The source of the hydrogen has been directly correlated with the injected silane by isotopic labeling experiments.[53] These observations can be explained by either H brought to the surface by precursor species or water intake since the model shows that the source of hydrogen in both cases can be attributed to the injected silane, and not necessarily impurities.

The deposition rate of SiO_2 for these conditions is 10–100 Å/min. This requires a flux of Si bearing precursors of $(20\text{–}200\times 10^{12})/r_s$ cm^2 s^{-1} where r_s is the reactive sticking coefficient. This implies a precursor density in the vicinity of the substrate of $\approx 2\times 10^9/r_s$ cm^{-3}. Since SiH_3, SiH_3O, SiH_2O, and HSiO all satisfy this requirement for reasonably large r_s (>0.01), and there is an abundant flux of O atoms, the results presented thus far are inconclusive as to the identity of the deposition precursor.

System studies have been performed by Lucovsky[56] for the deposition rate of SiO_2 as a function of SiH_4 flow rate, power deposition, and nozzle position. Parameterization of the model while varying these quantities may lend some insight to possible gas-phase precursors. We first parameterized the position of the nozzle. A subset of the results are in Fig. 5 where the densities of SiH_3 and SiH_2O are shown. As the nozzle is retracted from the substrate toward the plasma zone, the production of SiH_3 moderately increases as shown in Fig. 5(a). This results from the silane being injected into a region having a higher O atom density [see Fig. 3(a)]. Since the gas mixture is lean in SiH_4, the O atom flux is not significantly affected by the location of the nozzle. In spite of the increase in SiH_3 production, the flux of SiH_3 to the substrate decreases as the nozzles are retracted. This trend is a consequence of the SiH_3 having a greater opportunity to react away prior

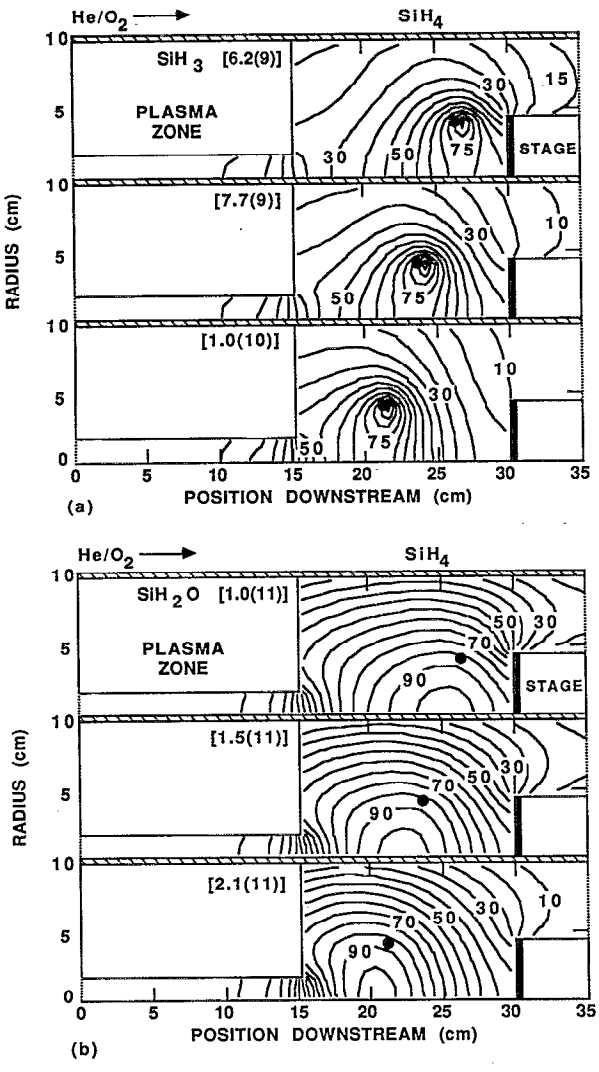

FIG. 5. Precursor densities for different nozzle positions for injecting SiH_4; (a) SiH_3 and (b) SiH_2O. The conditions are otherwise the same as Fig. 3. Although the maximum density of these species increases as the nozzle is retracted from the plasma zone, a smaller fraction survives to strike the substrate. (The labeling scheme is the same as for Fig. 3.)

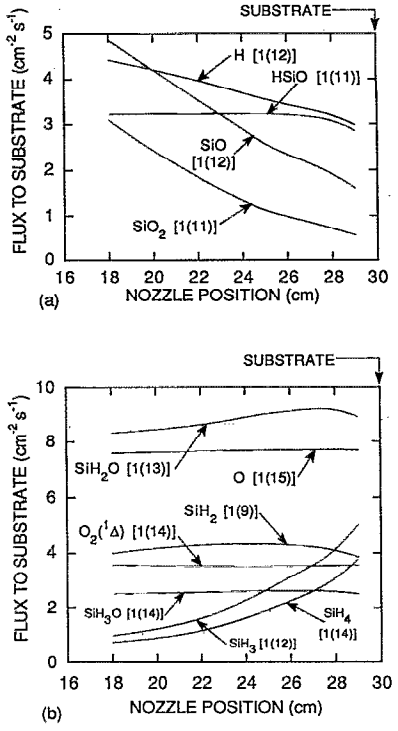

FIG. 6. Fluxes of deposition precursors to the substrate as a function of nozzle position for the base case conditions: (a) fluxes which decrease as the nozzle approaches the substrate; (b) fluxes which increase (or are constant) as the nozzle approaches the substrate. The numbers in brackets are the multiplying factor for the flux scale. The dependence of the higher-order precursors (HSiO, SiO, SiO_2) does not agree with experimental trends.

to reaching the substrate (primarily reacting with O_2 and sticking to the walls) when the nozzles are far from the wafer. A larger proportion of SiH_3 is also pumped away before striking the wafer when it is initially produced far from the substrate. The densities of SiH_2O show similar trends to SiH_3 when the nozzle is retracted from the plasma, as shown in Fig. 5(b). The production of SiH_2O increases when the SiH_4 is injected into a region of higher O atom density (where the SiH_3 also has a large density), however less of the SiH_2O survives to reach the substrate.

The fluxes to the substrate for various deposition precursors as a function of nozzle position are shown in Fig. 6. The experimental observation is that the deposition rate is a maximum for a nozzle position ≈ 2 cm above the substrate; with a linear decrease in deposition rate as the nozzle moves away from the substrate.[56] Two classes of radicals are shown: radicals whose fluxes decrease as the nozzle approaches the substrate [Fig. 6(a)] and radicals whose fluxes are nearly constant or increase as the nozzle approaches the substrate [Fig. 6(b)]. The fluxes of the higher-order precursors (HSiO, SiO, and SiO_2) decrease when moving the nozzle toward the substrate. This behavior is a consequence of SiH_4 being injected into a region of higher O atom density at distant nozzle positions. Production of precursors requiring multiple reactions with O atoms are thereby enhanced. The dependence of the fluxes to the substrate as a function of nozzle position for these species is the opposite of that experimentally observed for deposition rate. These results imply that is unlikely that HSiO, SiO, and SiO_2 are direct gas-phase deposition precursors.

More likely gas-phase deposition precursors are shown in Fig. 6(b). Only the fluxes of SiH_3 and SiH_4 directly scale in the same manner as the experimental deposition rate. Since the fluxes of $O_2(^1\Delta)$ and O atoms to the substrate are large, and not rate limiting, this scaling supports the proposal that surface catalyzed reactions between O [or $O_2(^1\Delta)$] and SiH_n are deposition precursors. The fluxes of SiH_2O and SiH_3O depend weakly on the position of the nozzle. Producing these species requires only a single reaction of O with SiH_4 (followed by a rapid reaction of SiH_3 with plentiful O_2). They also are not very sticky on surfaces. Their fluxes to the substrate therefore primarily de-

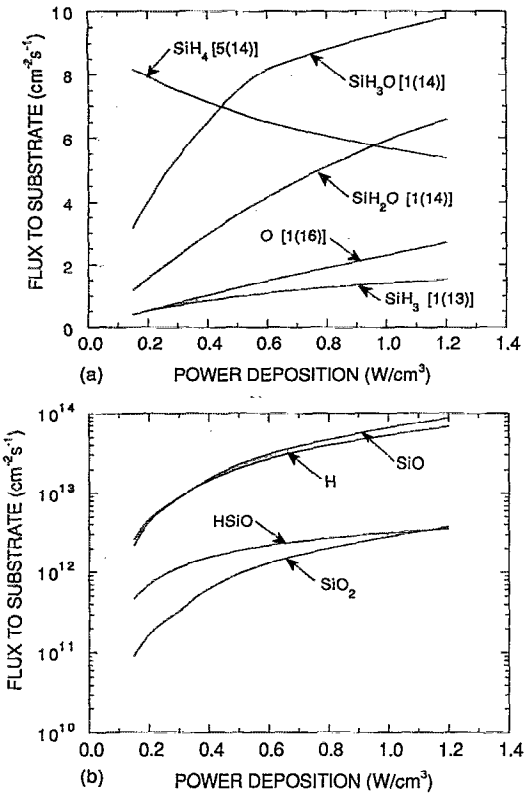

FIG. 7. Fluxes of deposition precursors to the substrate as a function of power deposition for the base conditions (the numbers in brackets are the multiplying factors for the flux scale): (a) Lower-order precursors; (b) higher-order precursors. The exponential increase in the flux of the higher-order precursors does not agree well with experimental trends for deposition rate.

pend on the reactor averaged total production of O, the partial pressure of SiH_4, and the flow patterns in the reactor.

Radical and molecular fluxes to the substrate are shown in Fig. 7 as a function of power deposition in the plasma zone. The production of O atoms, and their flux to the substrate, scale almost linearly with power deposition. The flux of SiH_4 to the substrate decreases with increasing power deposition as it is depleted by reaction with the larger density of O atoms. The production of SiH_3 and SiH_2O is somewhat less than linear with power as a result of this depletion. Species whose production requires many oxidation and elimination steps, such as HSiO, SiO_2 and SiO, rise exponentially with power deposition. The experimental observations are that the film deposition rate increases sharply at low power deposition and then becomes nearly constant.[56] SiH_3O, whose flux begins to saturate with increasing power, mimics the experimental observations of deposition rate. The exponential increase in the fluxes of higher-order products (HSiO, SiO, SiO_2) do not correlate well with the experimental observations for deposition rate. The fluxes of O and $O_2(^1\Delta)$ to the substrate increase with power deposition while the flux of SiH_4 decreases so that their product is nearly constant. This trend is similar to experiments, and supports the proposal that deposition results from surface catalyzed processes. Since,

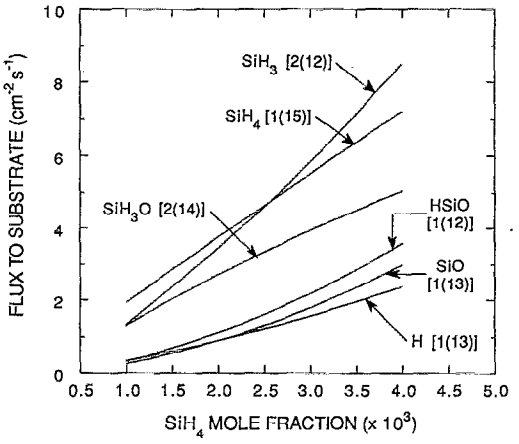

FIG. 8. Fluxes of deposition precursors to the substrate as a function of silane mole fraction for the base case conditions. The numbers in brackets are the multiplying factor for the flux scale. The lower-order precursor fluxes increase linearly with the silane flow rate.

however, the O atom flux is not rate limiting, the deposition rate should scale with the SiH_4 flux, which by decreasing does not correlate well with the experiments.

The fluxes to the substrate of various deposition precursors as a function of SiH_4 flow rate are shown in Fig. 8. The experimental observation is that deposition rate increases nearly linearly with SiH_4 flow rate over this range.[56] The fluxes of SiH_4, SiH_2O, and SiH_3O increase almost linearly with flow rate, whereas those for SiH_3, HSiO, SiO, and H increase somewhat greater than linearly with flow rate. The fluxes of O atoms and $O_2(^1\Delta)$ to the substrate are either constant or decrease slightly with increasing flow rate. The almost linear dependence of the fluxes of SiH_2O and SiH_3O to the substrate correlate well with the experimental observations of deposition rates. The dependence of the fluxes of Si bearing molecules to the substrate as a function of flow rate are inconclusive with respect to the identity of the deposition precursor since they scale similarly. Although the fact that the O and $O_2(^1\Delta)$ fluxes to the substrate decrease, or do not increase, with increasing silane flow rate, does not necessarily discount the surface catalyzed process since it is most likely rate limited by the availability of the silicon bearing precursors.

The radial distributions of precursor fluxes to the substrate are shown in Fig. 9 for our base case conditions. The edge-to-center uniformity of the low sticking coefficient precursors is 80%–90%. Their uniformity is dominantly determined by the flow pattern of the feedstock gases. Flow through the annular pumping port surrounding the substrate is the largest loss for low sticking coefficient species. Therefore, in spite of having low sticking coefficients, the "sink" of species beyond the edge of the wafer causes a center-to-edge gradient. An exception to this radial distribution pattern is the flux of $O_2(^1\Delta)$ which, for these results, is deactivated with unity probability on the substrate. This represents a sink for the $O_2(^1\Delta)$ which reduces the flux of $O_2(^1\Delta)$ at inner radii in a similar manner as radicals consumed in etching processes produce a "bull's-eye" etch-

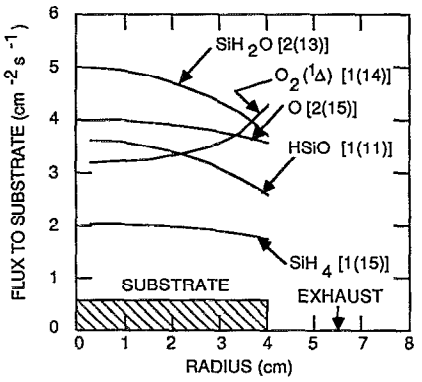

FIG. 9. Predicted fluxes of precursor species to the substrate as a function of radius on the substrate. The numbers in brackets are the multiplying factor for the flux scale. The center-to-edge profiles [for species other than $O_2(^1\Delta)$] results from the fluid flow patterns which exhaust gases in an annulus around the substrate. The unity quenching coefficient for $O_2(^1\Delta)$ on the substrate produces an inverted bull's-eye pattern.

ing pattern. A key diagnostic for determining whether deposition precursors include electronically excited species having high quenching coefficients on the surface is the center-to-edge uniformity of the deposition.

The gas-phase contribution of $O_2(^1\Delta)$ to producing deposition precursors by reaction with SiH_4 [Eq. (18)] was investigated by parameterizing its rate coefficient between 0 and 5×10^{-12} cm^3 s^{-1}. An example of the results are shown in Fig. 10, where the fluxes to the substrate for SiH_2O, SiH_3O, and $O_2(^1\Delta)$ are shown with and without the reaction in Eq. (18). The production of SiH_3O is more than doubled by the test reaction of $O_2(^1\Delta)$ with SiH_4. The production of SiH_2O increases by $\simeq$20% due to the reaction of O atoms with the larger density of SiH_3O. The flux of $O_2(^1\Delta)$ to the substrate decreases by $\simeq$25% as a result of the additional gas-phase reaction. Unless the rate coefficient for reaction of $O_2(^1\Delta)$ with SiH_4 approaches gas kinetic, an unlikely scenario, production of precursors by this process is not particularly important.

The use of $He/N_2O/SiH_4$ gas mixtures generally produces films which have less $\equiv$Si-OH bonding and, for otherwise identical conditions, have lower deposition rates by approximately a factor of 2.[53] The products of electron-impact dissociation of N_2O are primarily $O(^3P)$ and N_2 with minor amounts of $N_2(A)$ and $O(^1D)$. The fluxes of $N_2(A)$ and $O(^1D)$ which survive to reach the substrate are low, since both species are rapidly quenched by reactions with N_2O and SiH_4. The quenching of $N_2(A)$ on N_2O is dissociative, and produces additional O atoms. $O_2(^1\Delta)$ is not directly produced by electron impact of feedstock gases in the $He/N_2O/SiH_4$ system. The oxygen atoms that are produced can, however, recombine to produce O_2. The oxygen can, in turn, be excited to $O_2(^1\Delta)$ by electron impact or by excitation transfer from $O(^1D)$. In confined plasma configurations, sufficiently energetic electrons to excite the oxygen are only found in the upstream plasma zone, and so the production of $O_2(^1\Delta)$ by this sequence of events is low. These conditions reduce the likelihood that a surface catalyzed reaction between SiH_4 and $O_2(^1\Delta)$ is a direct deposition precursor using $He/N_2O/SiH_4$ chemistry.

The densities of O, SiH_3, HSiO, and SiH_2O are shown in Fig. 11 when passing a He/N_2O mixture through the plasma zone and injecting SiH_4 downstream. For these results, we have not included the reaction between SiH_3 and $N_2O(v)$ [Eq. (23)]. The conditions are otherwise the same as for the $He/O_2/SiH_4$ chemistry. The fluxes of precursor species to the substrate for the $He/N_2O/SiH_4$ [with and without the reaction in Eq. (23)] and $He/O_2/SiH_4$ chemistries are shown in Fig. 12. The spatial distributions of these precursor species using the $He/N_2O/SiH_4$ chemistry are similar to those obtained using the $He/O_2/SiH_4$ chemistry. The most striking differences are in the magnitude of the densities. The production of O atoms from N_2O (for the same power deposition and flow rate) is smaller by $\simeq$4–5, resulting in a proportionally smaller flux of O atoms to the substrate. The lower production of O atoms results from a larger proportion power being dissipated by vibrational excitation of N_2O and a lower rate of direct electron-impact dissociation compared to O_2.

As a consequence of the lower O atom density, the rate of H abstraction from silane by O atoms is smaller, resulting in a lower generation of SiH_3. However, SiH_3 is unre-

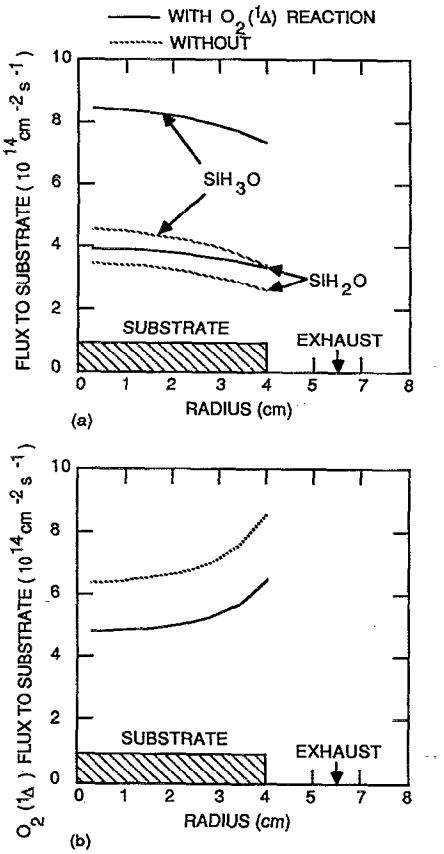

FIG. 10. Fluxes of deposition precursors to the substrate including and excluding the reaction $O_2(^1\Delta)+SiH_4\rightarrow SiH_3O+OH$: (a) SiH_3O and SiH_2O; (b) $O_2(^1\Delta)$. With a rate coefficient of 5×10^{-11} cm^3 s^{-1}, this reaction can account for a factor of 2 increase in the flux of SiH_3O and 25% decrease the flux of $O_2(^1\Delta)$.

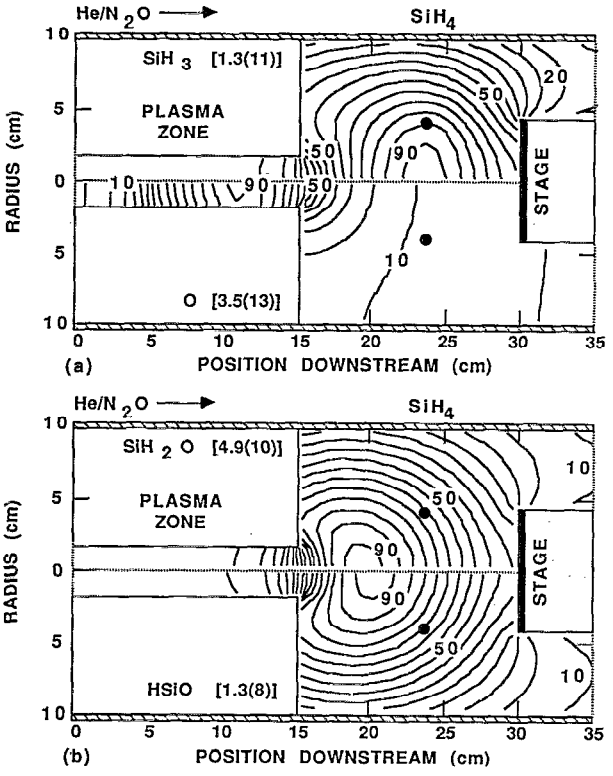

FIG. 11. Precursor densities when using $He/N_2O/SiH_4$ chemistry ($He/N_2O/SiH_4$=95/5/0.1, 300 mTorr, 220 sccm): (a) O and SiH_3; (b) HSiO and SiH_2O. Since SiH_3 is unreactive with N_2O, the density of SiH_3 is larger compared to using $He/O_2/SiH_4$ while the densities of HSiO and SiH_2O are smaller. (The labeling scheme is the same as for Fig. 3.)

active with N_2O at the temperatures of interest. This results in SiH_3 not being rapidly depleted by reactions with the feedstock gases, as it is with the $He/O_2/SiH_4$ chemistry. Therefore, SiH_3 ultimately has a larger flux to the substrate using the $He/N_2O/SiH_4$ chemistry. The fact that SiH_3 is not reactive with N_2O results in the only direct entrance channel to production of silanols being oxidation of SiH_3 by O atoms, which produces SiH_2O. A second-order entrance channel is reaction of SiH_3 with O_2 which has formed by recombination of O atoms. The production of SiO is smaller by approximately 10^2, and that of SiO_2 by 10^5 using the $He/N_2O/SiH_4$ chemistry. The former is a

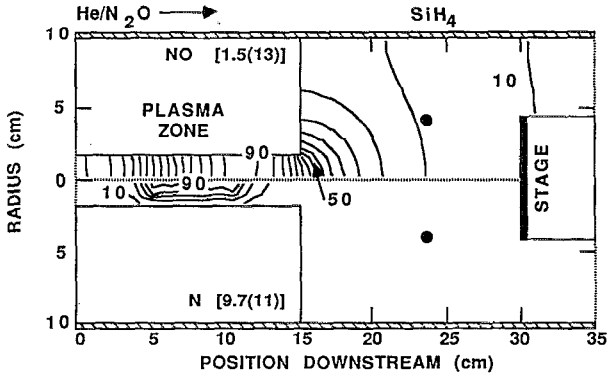

FIG. 13. Densities of N and NO for the conditions of Fig. 11. These species are largely unreactive with SiH_4. (The labeling scheme is the same as in Fig. 3.)

consequence of the lower densities of O and HSiO. The latter is a consequence of a low rate of reaction between SiH and O_2 using the $He/N_2O/SiH_4$ chemistry.

A unique feature of the $He/N_2O/SiH_4$ compared to the $He/O_2/SiH_4$ chemistry is the production of nitrogen species. For example, the densities of N and NO are shown in Fig. 13. The N atom density is $\simeq 10^{12}$ cm^{-3} in the plasma zone, generated in large part by dissociative ionization of N_2O producing $NO^+ + N$ and $N^+ + NO$. (N^+ recombination on walls then produces N atoms). These processes, as well as N abstraction from N_2O by $O(^1D)$, generate densities of NO exceeding 10^{13} cm^{-3}. The N atoms are largely consumed by reaction with the NO, producing $N_2 + O$. Once NO exits the plasma zone, however, it is relatively unreactive with most species except SiH. This reaction is a moderately important source of SiO and NH.

All of the nitrogen species in their ground electronic states are unreactive with silane. $N_2(A)$, which is reactive with SiH_4, is produced in large quantities, but is also rapidly quenched by collisions with N_2O and does not penetrate far downstream. A similar sequence of events occurs for $N(^4D)$; a species that is reactive with SiH_4 but does not penetrate far downstream. An important distinction between our test conditions and low-pressure RPACVD (tens of mTorr as opposed to hundreds of mTorr), uncon-

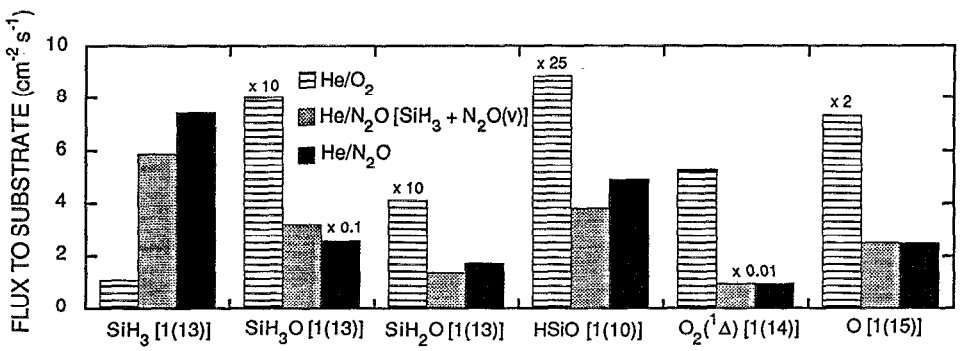

FIG. 12. Fluxes of precursors to the substrate when using $He/O_2/SiH_4$ and $He/N_2O/SiH_4$ chemistries. Values are shown for including and excluding the reaction of SiH_3 with $N_2O(v)$. The numbers in brackets are multipliers for the flux scale.

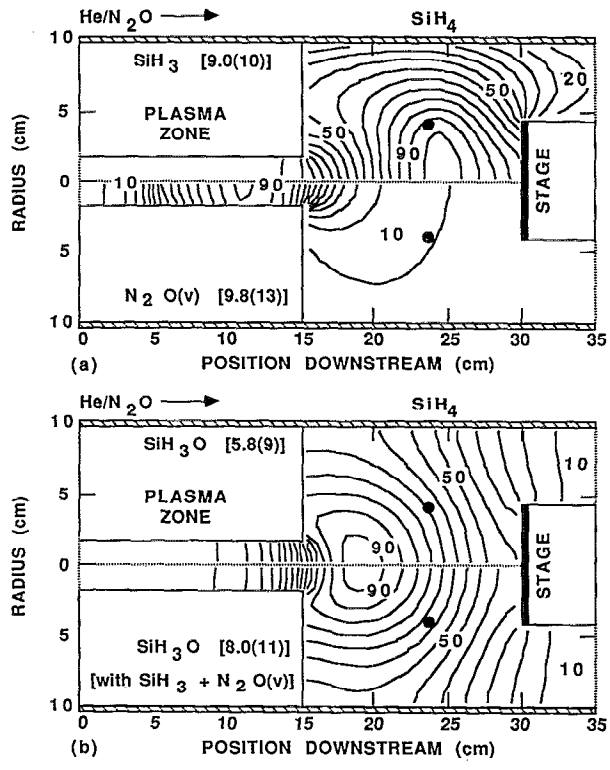

FIG. 14. Predicted densities when using $He/N_2O/SiH_4$ chemistry: (a) SiH_3 and $N_2O(v)$ and (b) SiH_3O. Values are shown for SiH_3O when including and excluding the reaction $SiH_3+N_2O(v)$. The density of SiH_3O is sensitive to this process since SiH_3 is unreactive with $N_2O(v=0)$. (The labeling scheme is the same as in Fig. 3.)

fined RPACVD plasmas, and direct PECVD is the mixing of these excited states of nitrogen with SiH_4. In the latter cases, production of NH species will be significantly higher.

Since SiH_3 is not reactive with ground-state N_2O, an important reaction channel is closed for production of silanol precursors. As a test, we included reaction of SiH_3 with vibrationally excited N_2O [Eq. (23)] as an entrance channel which produces SiH_3O (see discussion in Sec. III). The densities of SiH_3, $N_2O(v)$ and SiH_3O (with and without the test reaction) are shown in Fig. 14. The electron-impact cross sections for vibrational excitation of $N_2O(v)$ are large, resulting in $>10\%$ of N_2O being so excited. With the test reaction, the density of SiH_3 is depleted by $\simeq 50\%$. The production of SiH_3O increases by approximately a factor of 20; and so the test reaction is an important source of this precursor.

The fluxes of various deposition precursors to the substrate using $He/O_2/SiH_4$ and $He/N_2O/SiH_4$ [with and without the test reaction of $SiH_3+N_2O(v)$] chemistries are shown in Fig. 12. The experimental observation is that the deposition rate of SiO_2 using the $He/N_2O/SiH_4$ chemistry is $\geqslant 2$ times smaller than for the $He/O_2/SiH_4$ chemistry for otherwise similar conditions.[53] Due to the small density of O_2 produced with the $He/N_2O/SiH_4$ chemistry, the flux of $O_2(^1\Delta)$ to the substrate (produced by electron impact of O_2 in the plasma zone) is $\simeq 500$ times smaller than with the O_2 chemistry. The flux of SiH_4 to the substrate is nearly the same in all cases. If the deposition occurs by a surface catalyzed reaction of $O_2(^1\Delta)$ and SiH_4, the rate of deposition may well be rate limited by availability of $O_2(^1\Delta)$ with the N_2O chemistry. The flux of SiH_3 to the substrate is lowest using the O_2 chemistry, since SiH_3 is reactive with O_2, and largest for the N_2O chemistry when excluding reactions of SiH_3 with $N_2O(v)$. There is a small reduction in the SiH_3 flux when including this reaction.

Since SiH_3 is unreactive with N_2O, the production of SiH_3O and SiH_2O occur on only a radical-radical basis using the $He/N_2O/SiH_4$ chemistry. The production of these species and their fluxes to the substrate are greatly reduced compared to the $He/O_2/SiH_4$ chemistry, as shown in Fig. 12. When including reaction of SiH_3 with $N_2O(v)$, a portion of the SiH_3O production is recouped, but the flux of this precursor is still small compared to the $He/O_2/SiH_4$ chemistry.

These comparisons of precursor fluxes between the $He/O_2/SiH_4$ and $He/N_2O/SiH_4$ chemistries show large differences in the fluxes of SiH_2O, SiH_3O, and $O_2(^1\Delta)$, while the fluxes of SiH_3 and O are comparable. These results suggest that SiH_3 and O are likely deposition precursors, and that $=$Si-O bonds are formed on the surface as opposed to being produced in the gas phase.

V. CONCLUDING REMARKS

The production and fluxes of gas-phase deposition precursors during RPACVD of SiO_2 using $He/O_2/SiH_4$ and $He/N_2O/SiH_4$ chemistries have been investigated using a two-dimensional plasma chemistry model. Production of gas-phase precursors which have Si-O bonding (e.g., SiH_3O, SiH_2O, HSiO, SiO, and SiO_2) have been compared to production of $O_2(^1\Delta)$ which may be a reactant in a surface catalyzed process producing deposition. With $He/O_2/SiH_4$ chemistries, the fluxes of SiH_3O, SiH_2O, and SiH_3 to the substrate are sufficiently large to account for the observed deposition rates. However, systematic dependencies of the fluxes for HSiO and SiO, as well as their absolute magnitudes, discount these species as being precursors. The flux of $O_2(^1\Delta)$ to the substrate, in conjunction with SiH_4 (or SiH_3) is generally high enough to account for deposition by a surface catalyzed reaction. However, the flux of $O_2(^1\Delta)$ when using $He/N_2O/SiH_4$ is 100–500 times smaller than when using $He/O_2/SiH_4$ chemistries while the deposition rates are comparable. This tends to discount $O_2(^1\Delta)$ as being a dominant deposition precursor in both systems. Systematic dependencies of these fluxes suggest that SiH_3 (in the presence of a non-rate-limiting flux of O atoms) with contributions from SiH_2O and SiH_3O are likely gas-phase deposition precursors.

ACKNOWLEDGMENTS

The author would like to thank P. Westmoreland, G. Lucovsky, R. Markunas, and N. Masnari for their comments and advice. This work was supported by the Semiconductor Research Corporation, the National Science Foundation (ECS91-09326, CTS91-13215), IBM East

Fishkill Facility, and the University of Wisconsin Engineering Research Center for Plasma Aided Manufacturing.

[1] K. F. Jensen and W. Kern, in *Thin Film Processes II*, edited by J. L. Vossen and W. Kern (Academic, Boston, 1991), pp. 317–323.
[2] A. C. Adams, F. B. Alexander, C. D. Capio, and T. E. Smith, J. Electrochem. Soc. **128**, 1545 (1981).
[3] J. Batey, E. Tirney, J. Stasiak, and T. N. Nguyen, Appl. Surf. Sci. **39**, 1 (1989).
[4] J. Batey and E. Tierney, J. Appl. Phys. **60**, 3136 (1986).
[5] D. Eagle and W. I. Milne, Thin Solid Films **147**, 259 (1987).
[6] T. Fukuda, M. Ohue, N. Momma, K. Zuzuki, and T. Sonobe, Jpn. J. Appl. Phys. **28**, 1035 (1989).
[7] H. Gokan, A. Moritomo, and M. Murahata, Thin Solid Films **149**, 85 (1987).
[8] M. Kitagawa, T. Hirao, T. Ohmura, and T. Izumi, Jpn. J. Appl. Phys. **28**, L1048 (1989).
[9] G. Lucovsky, D. Tsu, R. Rudder, and R. Markunas, in *Thin Film Processes II*, edited by J. L. Vossen and W. Kern (Academic, Boston, 1991), pp. 565–619, and references therein.
[10] D. V. Tsu, G. N. Parsons, G. Lucovsky, and M. W. Watkins, J. Vac. Sci. Technol. A **7**, 1115 (1989).
[11] D. V. Tsu, G. N. Parsons, and G. Lucovsky, J. Vac. Sci. Technol. A **6**, 1849 (1988).
[12] G. Lucovsky, D. V. Tsu, S. S. Kim, R. J. Markunas, and G. G. Fountain, Appl. Surf. Sci. **39**, 33 (1989).
[13] D. V. Tsu, S. S. Kim, J. A. Theil, C. Wang, and G. Lucovsky, J. Vac. Sci. Technol. A **8**, 1430 (1990).
[14] J. A. Theil, D. V. Tsu, M. W. Watkins, S. S. Kim, and G. Lucovsky, J. Vac. Sci. Technol. A **8**, 1374 (1989).
[15] G. Lucovsky, J. T. Fitch, D. V. Tsu, and S. S. Kim, J. Vac. Sci. Technol. A **7**, 1136 (1989).
[16] G. Lucovsky and D. V. Tsu, J. Cryst. Growth **86**, 804 (1988).
[17] G. Lucovsky, P. D. Richard, D. V. Tsu, S. Y. Lin, and R. J. Markunas, J. Vac. Sci. Technol. A **4**, 681 (1986).
[18] G. Lucovsky and D. Tsu, J. Vac. Sci. Technol. A **5**, 2231 (1987).
[19] P. G. Pai, S. S. Chao, Y. Takagi, and G. Lucovsky, J. Vac. Sci. Technol. A **4**, 689 (1986).
[20] J. A. Theil, D. V. Tsu, and G. Lucovsky, J. Electron. Mater. **19**, 209 (1990).
[21] M. J. Kushner, J. Appl. Phys. **71**, 4173 (1992).
[22] M. J. Kushner, J. Appl. Phys. **63**, 2532 (1988).
[23] A. V. Phelps, Joint Institute for Laboratory Astrophysics Report No. 28, 1985.
[24] B. Eliasson and U. Kogelschatz, J. Phys. B **19**, 1241 (1986).
[25] A. V. Phelps and L. C. Pitchford, Phys. Rev. **31**, 2932 (1985), and references cited therein.
[26] M. Hayashi and A. Niwawi, in *Gaseous Dielectrics V*, edited by L. G. Christophorou and D. W. Bouldin (Pergamon, New York, 1987), pp. 27–32.
[27] L. E. Kline, W. D. Partlow, R. M. Young, R. R. Mitchell, and T. V. Congedo, Trans. Plasma Sci. **19**, 278 (1991).
[28] J. B. A. Mitchell, Phys. Rep. **186**, 215 (1990).
[29] G. R. A. Johnson, *Radiation Chemistry of Nitrous Oxide Gas*, NSRDS-NBS 45, 1973.
[30] J. T. Moseley, R. E. Olson, and J. R. Peterson, Case Stud. At. Phys. **5**, 1 (1975).
[31] S. Hadj-Ziane, B. Held, P. Pignolet, R. Peyrous, and C. Coste, J. Phys. D **25**, 677 (1992).
[32] W. B. DeMore, S. P. Sander, D. M. Golden, M. J. Molina, R. F. Hampson, M. J. Kurylo, C. J. Howard, and A. R. Ravishankara, Chemical Kinetics and Photochemical Database for Atmospheric Modeling, JPL Publication 90-1, 1990.
[33] W. Tsang and R. F. Hampson, J. Phys. Chem. Ref. Data. **15**, 1087 (1986).
[34] K. Tokuhashi, S. Horiguchi, Y. Urano, M. Iwasaka, H. Ohtani, and S. Kondo, Combust. Flame **82**, 40 (1990).
[35] F. Westley, J. T. Herron, R. J. Cvetanovic, R. F. Hampson, and W. G. Mallard, NIST Chemical Kinetics Data Base, Version 3.0, 1991.
[36] P. Dagaut, M. Cathonnet, J. C. Boettner, and F. Gaillard, Combust. Flame **71**, 295 (1988).
[37] C. DeJoseph, Report WRDC-TR-90-200, Wright Patterson Aero Laboratories, January 1990.
[38] L. G. Piper, J. Chem. Phys. **87**, 1625 (1987); **88**, 231 (1988).
[39] M. Kubo, M. Kogoma, T. Moriwaki, and S. Okazaki, J. Phys. B **22**, 3011 (1989).
[40] H. Koizumi, M. Ukai, Y. Tanaka, K. Shinsaka, and Y. Hatano, J. Chem. Phys. **85**, 1931 (1986).
[41] J. M. Pouvesle, A. Khacef, J. Stevefelt, H. Jahani, V. T. Gylys, and C. B. Collins, J. Chem. Phys. **88**, 3061 (1989).
[42] D. Albritton, At. Data. Nucl. Data Tables **22**, 8 (1978).
[43] L. G. Piper and G. E. Caledonia, J. Phys. Chem. **95**, 698 (1991).
[44] R. Atkinson and J. N. Pitts, Int. J. Chem. Kin. **10**, 1151 (1978).
[45] M. Petitjean, N. Proust, J.-F. Chapeanblance, and J. Perrine, Appl. Surf. Sci. **46**, 189 (1990).
[46] J. O. Chu, D. B. Beach, and J. M. Jasinski, Chem. Phys. Lett. **143**, 135 (1988).
[47] R. Becerra, H. M. Frey, B. P. Mason, and R. Walsh, Chem. Phys. Lett. **185**, 415 (1991).
[48] M. Nemoto, A. Suzuki, H. Nakamura, K. Shibuya, and K. Obo, Chem. Phys. Lett. **162**, 467 (1989).
[49] W. D. Reents and M. L. Mandich, J. Chem. Phys. **96**, 4429 (1992).
[50] C. J. Guinta, J. D. Chapple-Sokol, and R. G. Gordon, J. Electrochem. Soc. **137**, 3237 (1990).
[51] D. L. Smith, J. Vac. Sci. Technol. A **11**, 1843 (1993).
[52] I. R. Slagle, J. R. Bernhardt, and D. Gutman, Chem. Phys. Lett. **149**, 180 (1988).
[53] G. Lucovsky, D. Tsu, and R. Markunas, in *Handbook of Plasma Processing Technology*, edited by S. M. Roesnagel, J. J. Cuomo, and W. D. Westwood (Noyes, New Jersey, 1990), Chap. 16.
[54] A video animation of the $He/O_2/SiH_4$ RPACVD system is available from the author. Please send a blank standard VHS cassette with your request.
[55] J. C. Greaves and J. W. Linnet, Trans. Faraday Soc. **55**, 1355 (1959).
[56] G. Lucovsky (unpublished).